THE JOURNAL OF PHYSICAL CHEMISTRY C

ARTICLE

pubs.acs.org/JPCC

Ultrafast Dynamics of the First Excited-State of Quasi Monodispersed Single-Walled (9,7) Carbon Nanotubes

Frank Hennrich,[†] Manfred M. Kappes,[*,†,‡] Melanie Klinger,[‡] and Andreas-Neil Unterreiner[*,‡]

[†]Institute of Nanotechnology and [‡]Institute of Physical Chemistry, Karlsruhe Institute of Technology (KIT), Karlsruhe, Germany

Supporting Information

ABSTRACT: Time-resolved two color pump/probe spectroscopy was used to unravel the dynamics of ultrafast decay occurring upon population of the first optical bright excitonic level (E_{11}) in quasi-monodispersed, polymer-wrapped, single-walled (9,7)-carbon nanotubes (SWNTs) in toluene at room temperature. After resonant E_{11} excitation, transfer of population to at least one optically dark level near E_{11} was observed to take place within the first picosecond. In addition, phonon-assisted E_{11}-excitation led to transients similar to those observed upon resonant E_{11}-excitation indicating ultrafast vibrational relaxation convoluted with the temporal resolution of 60 fs.

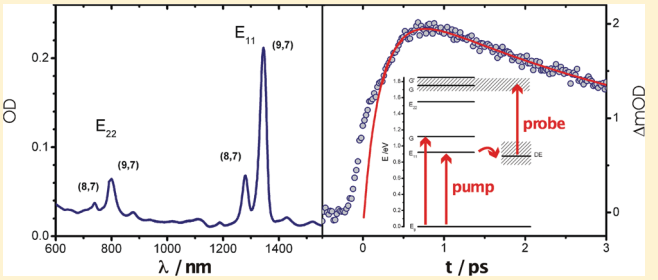

INTRODUCTION

The great variety of manufacturing and isolation methods used to prepare samples of purified single-walled carbon nanotubes (SWNTs) as well as the multitude of spectroscopic techniques applied to their characterization, have made it difficult to delineate relative contributions of the different processes involved in relaxation dynamics of SWNTs following electronic excitation. This has led, for example, to a wide range of experimentally determined excited-state lifetimes.[1−4] Often the SWNT samples studied comprised a mixture of different tube types with different chirality vectors (n,m) making the interpretation of intrinsic physical properties challenging. The presence of metallic SWNTs for instance can lead to quenching of the characteristic near-infrared fluorescence of electronically excited semiconducting nanotubes (s-SWNTs).[5] With improving purity of SWNT samples, new and sometimes surprising properties of SWNTs have been observed.[6,7] Recently, fluorenyl-based organic polymers have been used for the selection of specific tube types,[8] leading to near (n,m)-monodispersions of polymer-wrapped nanotubes (typically "solvated" in toluene). Such relatively pure samples can help to disentangle open questions regarding the electronic configuration in carbon nanotubes. The much better sample quality is often associated with an improvement in accuracy of (n,m)-specific physical measurements. Photoluminescence (PL) quantum yields of semiconducting single-walled carbon nanotubes (s-SWNTs) have correspondingly been remeasured and found to be somewhat larger (now on the order of 1%[8−10]) than previously thought. However, they are still too low for many applications. Such low fluorescence efficiencies are indicative of further pathways, which allow the nonradiative relaxation of optically excited SWNTs — eventually into their electronic ground state (GS). Very recently evidence has been obtained that suggests that quantum yields of up to 32% can be achieved by brightening SWNTs via exposure to reducing agents.[11] However, even then the major relaxation pathways would still remain nonradiative. These nonradiative relaxations can also occur via states that are only weakly optically accessible (= dark states) lying near the first optically allowed (= bright) exciton state, E_{11}. Analogously to similar materials like conjugated polymers, such dark states can be rationalized in terms of optically forbidden excitonic singlet states or triplet states.[12,13] In addition, phonon coupling effects can lead to a brightening of dark excitonic states, which can in turn give rise to sidebands in PL measurements.[6] In general, interaction between lattice modes and excited exciton states in a nanotube can result in energy transfer from the lattice to the exciton, or vice versa. This is known as exciton−phonon-coupling.[14] Two dark singlets and a dark triplet excitonic state have recently been inferred to lie close to the first bright exciton state of s-SWNTs. A zero momentum dark singlet exciton has been demonstrated to lie slightly below E_{11}.[15] A K-momentum dark singlet exciton lies somewhat above the bright exciton and can be observed in PL through its weak (temperature-dependent) emission from phonon sidebands (both above and below E_{11}). The dark triplet state is thought to lie somewhat below the bright exciton and is observed in PL in particular if trap states are present.[16,17]

In previous work on s-SWNTs, we first observed two weakly emissive intrinsic features present in PL spectra about 40 (DE_2) and 140 meV (DE_1), respectively, below the first bright exciton state, E_{11}.[18] We tentatively assigned these as "deep" dark excitonic states. In further investigations of such dark excitonic features in the PL of polymer-wrapped (9,7)-SWNTs in toluene

Received: August 5, 2011
Revised: October 19, 2011
Published: October 26, 2011

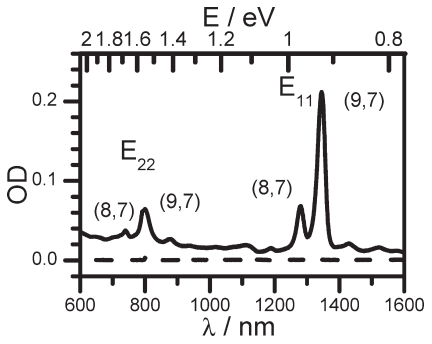

Figure 1. VIS-NIR spectrum of individualized (9,7)-SWNTs suspended in toluene/POF (solid line) together with a toluene/POF-solution reference measurement (dashed line). Both absorption spectra are background corrected with respect to toluene.

suspension, we have also explored G-phonon-coupled excitation and emission transitions.[9] Stimulated by recent studies that showed a strong temperature dependence of two (weak) PL features below E_{11}[16] we have returned to this problem. In particular, the case for assignment of DE_2 and DE_1 to triplet and (phonon coupled) singlet state excitons, respectively, would be supported further by measurements showing corresponding excited-state dynamics. Here we report on time-resolved transient absorption spectroscopy that helps us to identify the corresponding time scales, coupling mechanisms, and branching ratios after ultrashort photoexcitation of the first bright exciton state, E_{11}, in polymer-wrapped (9,7)-SWNTs.

EXPERIMENTAL SECTION

Sample Preparation. SWNTs were synthesized by laser ablation using a carbon composite rod containing a Ni/Co catalyst, pure Ar as process gas, and a furnace operating in the temperature range of 1420 K.[19] Accordingly, a characteristic distribution of nanotube species is obtained that comprises about 20 different semiconducting tube types.[20] The raw material was ultrasonically dispersed in toluene containing 0.1% by weight of poly[9,9-dioctylfluorenyl-2,7-diyl] (POF).[9] The polymer is both selective to certain (*n*,*m*)-species and used to prevent aggregation between the tubes. After ultracentrifugation to remove contaminants and bundles, the procedure leads to near monodispersed suspensions of semiconducting (9,7)-SWNTs with a minor contribution of (8,7)-tubes also present. The molar weight of a specific SWNT component can be estimated from PL and absorption spectra as well as the corresponding cross sections following the procedure used in ref 21. We determine a molar weight of ~80% for the dominant (9,7)-species from UV−vis-NIR-absorption spectroscopy (spectrum displayed in Figure 1; spectrometer: Varian Cary 5E; cuvette: fused silica with an optical path length of 1 mm) by comparing the OD values of the first optically allowed (bright) excitonic transitions, E_{11}, of (9,7)-tubes peaking at 1344 nm and (8,7)-tubes at 1280 nm, respectively. The second bright exciton transition, E_{22}, lies between 700 and 800 nm. The polymer POF shows only significant absorption in the near UV and does not interfere with pump−probe measurements of the (9,7)-tube in the infrared region. The pure POF-toluene reference absorption spectrum is also shown in Figure 1. In general, low background and sharp absorption peaks indicate a sample with unbundled and well-dispersed SWNTs without the presence of measurable amounts of metallic SWNTs or impurities like amorphous carbon particles.[8] To conduct time-resolved pump−probe-experiments, we stored the samples in a fused silica cell with an optical length of 1 mm. The optical density OD of the samples during the measurements was kept between 0.2 and 0.3 at the resonant E_{11} excitation wavelength of 1344 nm.

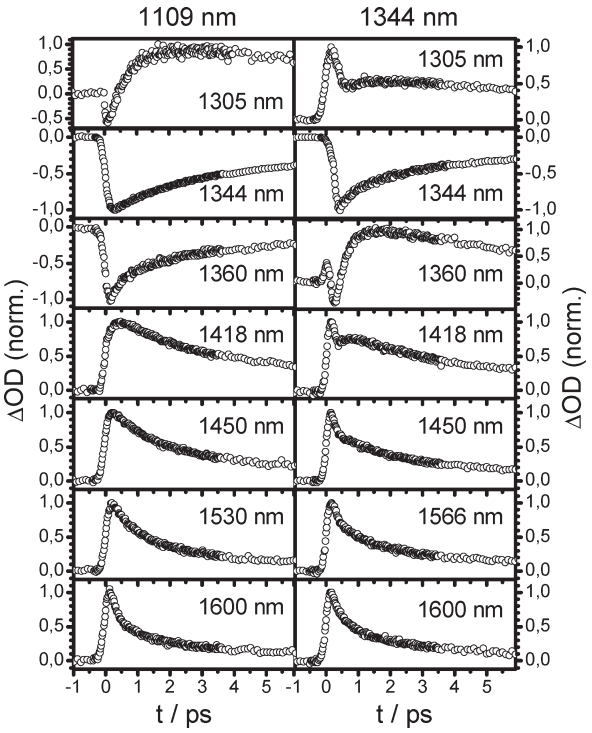

Figure 2. Representative temporal profiles of (9,7)-SWNTs in toluene/POF. Pump wavelengths are 1109 and 1344 nm, respectively, and probe wavelengths are as indicated. Data have been normalized to the respective maximum pump-induced absorption value.

Laser System. Time-resolved transient absorption measurements were carried out with a commercial 1 kHz amplified Ti:sapphire laser system (CPA2210, Clark-MXR) operating at a center wavelength of 775 nm. After frequency-doubling, this source served as a pump for two NOPAs (noncollinear optical parametric amplifier, Clark-MXR) independently tunable from about 450 to 1600 nm. The NOPAs provided wavelengths for both pump and probe pulses in the infrared region with an approximate spectral width of 50 nm and pulse duration of 60 fs. To monitor the time and wavelength-dependent change of the optical density, ΔOD, InGaAs-photodiodes (Hamamatsu, G8371-03) were used to record the infrared light of the probe pulse before and after radiation of the sample volume. The time delay between pump and probe pulse was accomplished by a computer-controlled translation stage (Physik Instrumente) with a time resolution of 0.67 fs. Pump and probe pulses were parallel-polarized with regard to each other.

The experiments were carried out under unfocused conditions with a beam diameter of the pump pulses of ~2 mm to avoid local heating and significant contributions from exciton−exciton−annihilation processes (requiring $>2 \times 10^{14}$ photons/(cm^2 pulse)[22−25]). Under our experimental conditions, the pump pulses did not exceed 5×10^{13} photons/(cm^2 pulse).

RESULTS

To examine the ultrafast dynamics of (9,7)-SWNTs, we resonantly excited the first bright exciton state E_{11} by a 1344 nm

Table 1. Time Constants τ_1, τ_2, and τ_3 and Relative Amplitude $RA(w_3) = w_3/(w_2 + w_3)$[a]

λ_{exc}	1109 nm				1344 nm			
λ_{probe} [nm]	τ_1 [fs]	τ_2 [ps]	τ_3 [ps]	$RA(w_3)$	τ_1 [ps]	τ_2 [ps]	τ_3 [ps]	$RA(w_3)$
1344		2.2	33	0.29	139	2.5	32	0.28
1430					84	1.8	24	0.28
1450		1.9	25	0.21	60	2.0	21	0.28
1530		1.6	22	0.22	67	1.6	19	0.21
1566		1.4	18	0.15	198	1.6	19	0.21
1600	100	1.6	26	0.22	304	2.1	21	0.18

[a] w_1 has not been considered because of its contribution of <5%.

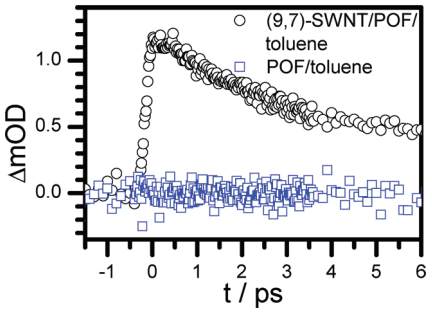

Figure 3. Temporal profile of (9,7)-SWNTs in POF/toluene (circles) compared with an analogous measurement for a POF/toluene solution (squares) at a pump−probe combination of 1109/1410 nm.

pump pulse. In a separate set of measurements, we also pumped at 1109 nm. This wavelength corresponded to a phonon-assisted transition involving (co)excitation of the so-called G-mode (at 1580 cm^{-1}), a well-known feature in Raman (and PL-) studies of carbon nanotubes.[26,27]

Figure 2 provides an overview of the time-resolved transients measured in the probe pulse regime at wavelengths between 1305 and 1600 nm. The panels on the left side show the transient profiles after 1109 nm excitation (E_{11} + G-band), and those on the right show the transient profiles after 1344 nm excitation (direct E_{11}), respectively. For ease of comparison, the profiles are normalized with respect to their first negative and positive peak ΔOD values, respectively. Only at probe wavelengths around 1344 nm do we observe transient bleaching. At all other wavelengths studied we observe strong or even dominant induced absorption (IA), which can in turn be attributed to the population of states, which are more strongly absorbing than the GS. A special feature can be seen at a probe wavelength of 1360 nm. Here transient bleaching (after 1344 nm excitation) is superimposed with an IA contribution of roughly equal magnitude. For the corresponding phonon-assisted excitation at 1109 nm, probing at 1360 nm reveals only bleach with a somewhat shorter recovery time than observed for the 1344 nm probe wavelength. This is again a consequence of an analogous superposition, a phenomenon that limits the accessible spectral window for bleach detection, in agreement with previous findings.[3,28]

Excitation at 1344 nm and probing at 1305 and 1418 nm result in transients that manifest a second maximum after roughly 1 to 2 ps. This is indicative of the time-resolved dynamics of one or more "dark" states in the vicinity of the E_{11} level of the (9,7)-tube.

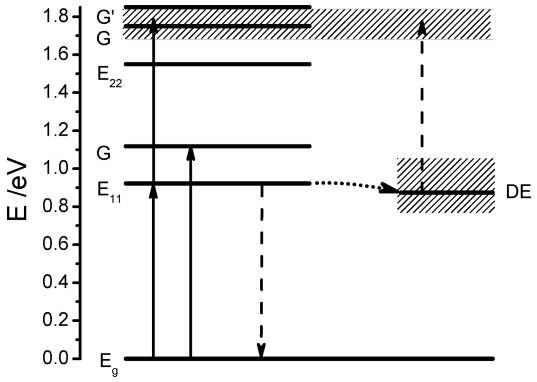

Figure 4. Simplified energy level diagram of a (9,7)-SWNT adapted from ref 9. (See the text for further details.) Nanotube excitation is represented by solid arrows, whereas the probe pulse is indicated by dashed arrows.

(See the Discussion.) At a pump−probe combination of 1109/1418 nm, this second maximum is much less pronounced than that in the case of 1344/1418 nm. The ultrafast temporal response observed around time zero (designated by τ_1 in Table 1) is not understood in detail. However, it is not important for the further discussion of the main results presented here. To exclude direct contributions of both the solvent and the polymer to the transient response, we also conducted time-resolved reference measurements of a POF/toluene-solution. (See Figure 3 for a typical pump−probe wavelength combination of 1109/1410 nm.)

Figure 4 shows a simplified energy level diagram of the (9,7)-SWNT based on that put forward by Kiowski et al. to rationalize their PL spectroscopic measurements.[18] These investigations revealed two weakly emissive features lying at about 792.5 and 874.5 meV, respectively, just below the first bright excitonic state E_{11} (922.5 meV).[2] These were attributed to dark exciton states, DE_1 and DE_2. Furthermore, the second bright exciton level, E_{22}, and Raman active G-modes and overtone G′-modes coupled to the bright electronic transitions are also shown in the Figure. Femtosecond excitation and probing are represented by continuous and dashed arrows, respectively. Relaxation of the E_{11} state into dark excitonic states (e.g., DE_1- and DE_2-states, indicated with a grayed area) is denoted with a dotted arrow. (The "DE_1" emission feature has since been shown to be due to a phonon-coupled sideband of the K-momentum dark exciton that lies slightly above E_{11}.) Because of the quasi-monodispersion of the sample, additional contributions to the transient response can only arise from the E_{11} transition of (8,7)-tubes. However, a 1344 nm-pulse with a full width at half-maximum (fwhm) of ∼50 nm cannot support excitation at ∼1280 nm (969 meV), which would be required to access the peak position of the E_{11} transition of the (8,7) tube (fwhm ca. 20 nm). The same consideration holds true for the phonon-assisted excitation of the E_{11}-state. Assuming the same energy of ∼200 meV for the G-mode excitation of both tube-species,[29,30] the exciton−phonon-coupled transition of the (8,7)-tube lies at 1060 nm and is not likely to be excited with a wavelength of 1109 nm.

On the basis of these considerations, the transients obtained after resonant as well as phonon-assisted E_{11}-excitation were evaluated by fitting the data to bi- and triexponential decays, respectively. In addition, transients were modeled by two kinetic schemes. (For details, see the Supporting Information.) Good

Table 2. Time Constants τ_r, τ_4, and τ_5 at Probe Wavelengths of 1305 nm and between 1380 and 1400 nm

λ_{exc} [nm]	1109			1344		
λ_{probe} [nm]	τ_r [ps]	τ_4 [ps]	τ_5 [ps]	τ_r [fs]	τ_4 [ps]	τ_5 [ps]
1305				0.9	2.4	26
1380	0.2	3.2	17	0.4	4.1	22
1400	0.2	3.1	15	0.4	3.4	22
1418	0.2	2.3	15	0.4	2.5	19

agreement between experiment and modeling could be achieved by taking into account extrinsic relaxation pathways. This indicates the need to incorporate trap states. It is worth noting, that the optimum evaluation method for the transients depends on the pump wavelength. Best results after 1109 nm excitation were obtained by fitting the transient absorption decay bi-exponentially, whereas after 1344 nm excitation best fits were obtained by applying a tri-exponential function. Table 1 lists the time constants τ_1, τ_2, and τ_3 as well as the relative amplitude $RA(w_3) = w_3/(w_2 + w_3)$ (neglecting the contribution of the relatively small amplitude of w_1 (<5%)). Additionally, the rise time and decay of those transients that show a second maximum were fitted to a monoexponential growth function and a biexponential decay function. The resulting time constants τ_r, τ_4, and τ_5 are listed in Table 2.

DISCUSSION

Excited-State Lifetime. Previous pump−probe measurements have often been plagued by the presence of multiple, spectrally overlapping (n,m)-types in the nanotube samples. Therefore, usually more than one nanotube species was excited. Exciton transitions were then typically probed off-resonantly[3] under conditions of overlapping IA and induced bleaching (IB) contributions from different nanotube species, thus considerably complicating the analysis.[31] Furthermore, it has been demonstrated[32] that the superimposed IA and IB contributions in such samples may not only be due to their polydispersive nature but may also reflect the nature of the individual nanotubes themselves. Because of the near monodispersion of the (9,7)-SWNTs used in the present work and by comparison with previous work on polydisperse suspensions, assignments of physical properties like excited-state lifetimes to a specific tube type can be accomplished more accurately.

One color pump−probe experiments were conducted at a wavelength of 1344 nm (922.5 meV), as depicted in Figure 5. The shortest time constant, τ_1, on the order of 100 fs, is of no relevance in this context and certainly not related to the intrinsic lifetime of the excited state but to cross correlation, [1 + 1] photon absorption contributions, residual contributions from exciton−exciton annihilation, or other (coherent) processes. At longer pump−probe time delays two more time constants $\tau_2 = (2.2 \pm 0.5)$ ps and $\tau_3 = (32 \pm 4)$ ps are obtained. The origin of a comparable time constant τ_2 observed in literature studies is generally linked to exciton degradation induced by bundling effects, to lower lying trap states (caused by defects in the lattice structure), or to optically dark excitonic states.[28,33,35] We note that our suspensions have extremely low bundle content because the polymer is selective for individual (9,7) nanotubes. Finally, the long time constant, τ_3, often is associated with the lifetime of

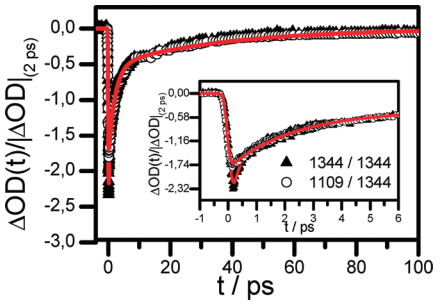

Figure 5. Normalized induced transient bleach of (9,7)-SWNTs in toluene/POF for 1344 and 1109 nm excitations while probing at 1344 nm. Symbols denote experimental values and solid lines represent the corresponding exponential fits. For better comparison, transients have been normalized to their absolute ΔOD values at 2 ps. Inset: transient profiles at short delay times.

the first bright electronic state, E_{11}.[3,34,35] According to Table 1, the time constants τ_2 and τ_3, probed in the wavelength regime between 1430 and 1600 nm, are comparable to the results at a probe wavelength of 1344 nm with a tendency toward smaller values for τ_3 with longer probe wavelengths in agreement with previous literature data.[36]

A major challenge in transient absorption measurements is the interpretation of time constants resulting from fits to the experimental data. In particular, in large molecules with a large variety of accessible excited states and subsequent pathways of relaxation this is because the transients often comprise different contributions and time constants. Therefore, transients typically cannot be assigned to just one single process or reaction sequence. If the transients at 1344/1344 nm, for example, are governed by GS bleaching, then τ_3 may contain not only the lifetime of the E_{11} state but also contributions of other states lying in the vicinity or beneath E_{11} as well, thus masking the lifetime of the first bright excited state. As a consequence, the transients were modeled kinetically to obtain a rough idea of the complex relaxation pathways pertaining in (9,7)-SWNTs. Modeling of the time-dependent excited-state population based on the assumptions made above supports an interpretation of our experimental data involving dark excitonic and trap states. As a result of this modeling, time constants τ_2 and τ_3 are indeed found to comprise combinations of rate constants from different relaxation processes. In particular, the assignment of τ_3 to the lifetime of E_{11} then strongly depends on the energy gap between bright, dark, or trap states as well as on individual decay rates. (See the Time-Resolved Population of Dark States section and the Supporting Information.)

Exciton−Phonon-Coupling. Another important aspect of the excited-state dynamics becomes apparent when (9,7)-SWNTs are off-resonantly excited. Specifically, if the pump-pulse is tuned to a wavelength corresponding to E_{11} plus G-mode, a so-called phonon-assisted excitation can be observed. Consequently, excitation at 1109 nm results in a photobleach transient at a probe wavelength of 1344 nm, much as is seen for direct resonant E_{11}-excitation. For better comparison, the transients for the pump−probe combination 1109/1344 and 1344/1344 nm are shown superimposed in Figure 5 (normalized to their absolute ΔOD-values at 2 ps). The analysis (Table 1) reveals almost identical values for the time constants τ_2 and τ_3. The only difference is the missing ultrafast component (τ_1) for 1109 nm excitation (E_{11} plus G-band). Moreover, the striking similarity of

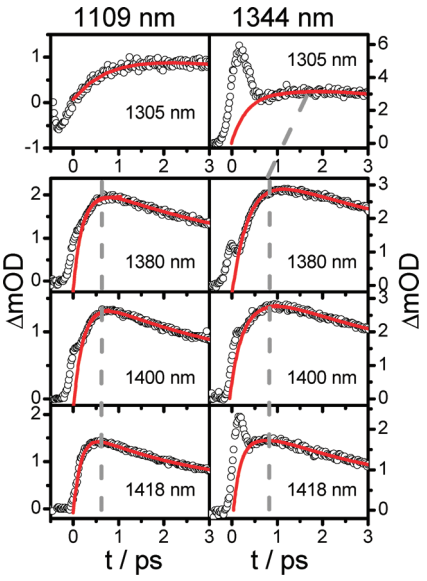

Figure 6. Temporal profiles of (9,7)-SWNTs in toluene/POF after excitation at 1109 nm (left) and 1344 nm (right) and obtained by probing between 1380 and 1418 nm. Rise and decay of the second maximum were fitted to a monoexponential growth function and a biexponential decay function. Fits are indicated as solid lines. The gray dashed line highlights the second maximum.

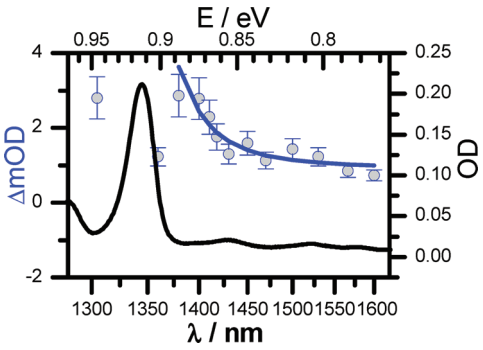

Figure 7. Stationary absorption spectrum (solid line, right axis) and transient spectrum of a (9,7)-SWNT in toluene/POF sample excited at 1344 nm after 0.8 ps (filled circles, left axis). The time delay between pump and probe was chosen to be in the second ΔOD maximum. The line only serves as guide for the eyes. The error is estimated to be roughly 20% of the ΔOD value taking into account variation of the pump/probe overlap as well as intensity fluctuations.

τ_2 and τ_3 can be observed for all probe wavelengths to the red of the peak position of the E_{11} transition. Even the relative amplitudes coincide for the combinations 1109/1344 nm and 1344/1344 nm, that is, 70% for component 2 and 30% for component 3, respectively. Obviously, both resonant and phonon-assisted excitations lead to comparable photoinduced processes. This result suggests that vibrational relaxation, caused by the coupling between G-mode and bright exciton, occurs within the temporal resolution of our setup (~60 fs). Theoretical calculations estimate a coupling time constant of ~90 fs for nanotubes surrounded by vacuum[29] and a coupling time constant of ~30 fs for tubes in bulk material.[37] Our upper limit of 60 fs for a measurement in condensed phase thus agrees well with these theoretical findings. The lack of the ultrafast component after phonon-supported excitation can be rationalized in terms of a lower excitation density of the pump pulse at 1109 nm. Along with a presumably smaller absorption cross section for the phonon-assisted excitation (compared with resonant conditions), this would cause a less efficiently populated E_{11} state, thus making those processes previously mentioned, which lead to the τ_1 component, less significant.

Time-Resolved Population of Dark States. In the spectral window between the probe wavelengths of 1305 and 1418 nm, we observe an additional second maximum in IA transients (Figure 6), both under resonant (right panel) and under phonon-assisted (left panel) excitation. For the purposes of this discussion, we will assume that this transient is governed by E_{11} depopulation to one or more "dark" states not seen in the stationary absorption spectrum, but which strongly absorb at the probe wavelength. In general, the corresponding absorption may arise from probe-induced excitation of this dark state into higher state(s) in the vicinity of the E_{22}-manifold including also G-phonon coupling (as indicated by dashed upward arrows in Figure 4). Excitation with 1109 nm (E_{11} + G-band excitation) results in negative ΔOD values around time zero and a positive maximum at later times, which is indicative of competing photoinduced processes in (9,7)-tubes. Because of this superposition, the maximum observed in the 1109/1305 nm transient is therefore not by itself a clear indicator of E_{11}-state transfer into a (lower lying) dark state. At a probe wavelength of 1418 nm, the temporal profile qualitatively resembles the profile at 1305 nm. Here a second maximum in the transient absorption arises between 0.6 and 1 ps (more clearly seen after resonant excitation). Again, this can be associated with the population of a dark state DE. Note that the energy difference of 70 meV between the probe wavelengths 1305 and 1418 nm roughly matches the experimentally determined energy gap between DE_1 and DE_2.[9] Assuming that both probe wavelengths take the respective intermediate dark states to the same final excited state, we could interpret the second maxima to be indicative of the population of DE_1 (1305 nm probe) or DE_2 (1418 nm probe), respectively.

Fitting of the corresponding transients (Table 2) results in two time constants, τ_r = 0.9 (for 1305 nm) and 0.4 ps (1418 nm), respectively. These time constants also seem to depend on the excitation energy. After photoexcitation of the phonon-assisted E_{11}-state, the resulting time constant is τ_r = 0.2 ps (1418 nm) and thus faster compared with resonant conditions (τ_r = 0.4 ps). Whether this faster population could be due to the dispersive nature of the G-band is not yet clear. According to this finding, there is no final evidence that there are indeed two differentiable dark states, DE_1 and DE_2, in this region. Figure 7 provides an overview of the IA (left ordinate) at a pump−probe time delay of 0.8 ps (i.e., in the vicinity of the second ΔOD-maximum) as a function of the probe pulse wavelength. This is compared with the stationary absorption spectrum of the SWNT/POF/toluene sample (right ordinate). In the region around the resonant E_{11}-excitation wavelength of the (9,7)-SWNT (1344 nm), bleach dominates the pump-IA spectrum and may mask higher state absorption contributions. The spectral dependence of the observed IA indicates that participating dark states have a peak absorption wavelength very near to E_{11}. In addition to τ_r, the biexponential fit provides two more time constants, τ_4 and τ_5 which are on the order of 3 and 20 ps respectively. Assuming that in fact two dark states are populated and eventually relax to the electronic GS, one might assign these two time constants to each of the two dark states. Again, kinetic modeling has been used to

dx.doi.org/10.1021/jp2075176 |J. Phys. Chem. C 2011, 115, 23711–23717

support our interpretation. The experimental transients have been modeled either by applying: (i) a three-level system, consisting of an excited excitonic bright state (B), a dark state (D), and the ground state (G) or (ii) a four-level system that takes extrinsic effects into account by adding a trap state to the previous three-level system (schemes 1 and 2 in the Supporting Information). An important parameter is the energy gap ΔE that controls the population transfer between dark and bright states. For an energy gap of 5 meV, for example, the rate constants for the transfer between bright and dark states are on the same order of magnitude. An energy gap of 140 meV, on the other hand, leads to a transfer rate back to the bright state that is slower by three orders of magnitude, making population back transfer more unlikely. Applying scheme 1 as well as scheme 2, the transients probed with 1305 and 1418, respectively, can be modeled at least qualitatively by involving a dark excitonic state lying energetically below E_{11}. It has been shown that extrinsic effects like trap states or environmental effects that depopulate E_{11} are crucial for a qualitatively satisfactory modeling of the experimental data, too. This is reasonable because the SWNTs in our sample are certainly subject to influences from the POF/toluene environment. Intrinsic pathways like relaxation into dark excitonic states lying below the E_{11} state may also play an important role in the relaxation behavior of excited nanotubes.

Direct time-resolved results for dark-state dynamics are generally difficult to interpret because bright-to-dark state excitation via one-photon absorption is usually not allowed, and subsequent relaxation of dark state population is always nonradiative. Because of this difficulty, the nature of the states that give rise to weak PL about 40 and 140 meV below E_{11} is still controversially discussed. Theoretical calculations have predicted the existence of at least one dark singlet exciton below E_{11} in SWNTs.[38−41] In agreement with Zhao et al.,[13,40] Kilina et al.[42] have predicted three dark singlet excitonic states to lie below the first bright singlet state. These could serve as trap states within the E_{11}-manifold. Recently, low-energy emission bands about 130 meV below E_{11} have been attributed to a phonon-coupled K-momentum dark exciton energetically slightly above E_{11},[6,43] Other experimental findings have associated this feature with "dark singlet excitonic states".[18] On the basis of low-temperature micromagneto-PL studies, Srivastava et al. have found unequivocal evidence for a zero-momentum dark singlet exciton state lying ca. 5 meV below the first bright exciton.[15] Zhu et al.[32] have performed time-resolved pump−probe-measurements on (6,5)-SWNT samples and have obtained transients that could be fitted to a $t^{-0.45}$ power law. This was attributed to subdiffusive trapping of dark singlet excitons. Relaxation from E_{11} into the lowest lying dark state was determined to occur with a time constant on the order of 6 ps. In contrast with our results, these authors obtained transient spectra after photoexcitation of E_{11} with blue-shifted IA with respect to the IB signal. This was assigned to excited-state absorption from the lowest dark state into the 2 E_{11}-manifold. No red-shifted IA, indicating trionic or biexcitonic states, was observed. Previous literature data revealed evidence of the formation of charged excitons by means of red-shifted IA.[44,45] Whereas we cannot completely rule out trionic behavior in (9,7)-SWNTs, the experiments were kept under low excitation density conditions, where the generation of trions should be relatively small. Biexcitons would equally induce red-shifted absorption spectra[46] but are excluded from our considerations for the same reasons as is the case of trions. Harutyunyan et al.[47] used time-resolved PL to identify dark states 130−150 meV below E_{11} in (6,4)- and (5,4)-SWNTs, by brightening the dark states through defect-induced mixing of states. They observed lifetimes of 65 and 177 ps depending on the energy gap between E_{11} and DE and related this to relaxation of (dark) triplet states. By comparison, here the time constant τ_3 was found to be on the order of 20 ps; that is, the corresponding dark state in our experiments does not appear to be quite as long-lived. In a recent PL study by Matsunaga et al.,[16] temperature-dependent measurements on different SWNT species have provided clear evidence of two different states associated with weak emission below E_{11}. On the basis of decreasing PL intensity with decreasing temperature, the emission feature observed in unperturbed s-SWNTs about 130 meV below E_{11}, was attributed to a phonon-coupled K-momentum dark exciton (with the corresponding singlet dark exciton lying at ca. 40 meV, slightly above E_{11}). The other state was preferentially observed for laser-defected nanotubes. It lies below E_{11} with an energy difference that is strongly dependent on diameter. On the basis of its increasing PL intensity with decreasing temperatures, it has been attributed to a triplet dark exciton state. One might expect dark triplet-, dark zero-momentum singlet-, and dark K-momentum singlet-exciton states close to E_{11} to be populated on very different time scales, for example, owing to the necessity for intersystem crossing from E_{11} into the triplet system. We do not see any indication of this. However, the relative detection efficiencies for these types of dark states may be quite different, thus perhaps discriminating against one or the other form. Furthermore, in our experiments, we were careful not to induce any photochemical damage, which may limit the singlet/triplet dark exciton branching ratio. Further efforts with well-defined, intentionally defected samples[17] and more sophisticated experimental tools may help to unravel this issue. At present, our results indicate strong transient absorption from dark state(s) populated within <1 ps after E_{11} excitation, but they do not allow an unambiguously clear assignment of the dark states' nature.

SUMMARY AND OUTLOOK

Time-resolved pump−probe experiments on semiconducting (9,7)-SWNTs, dispersed in POF/toluene, yielded new insight into the relaxation pathways of the first allowed exciton state E_{11}. Two-color investigations of a quasi- monodispersed SWNT-suspension of (9,7)-tubes in the near-infrared spectral region allowed the observation of dark-state population in the vicinity of the first bright exciton state, E_{11}. Depending on probe wavelengths, the dark state(s) are observed to be generated within 1 ps. Further investigations under nonresonant conditions clearly showed the existence and an upper limit for the time scale of the coupling of phonon-assisted transitions of the E_{11} state. Future efforts toward understanding the nature of dark state(s) accessed should focus on the investigation of other (n,m)-types as well on further improvements in sample preparation.

ASSOCIATED CONTENT

Supporting Information. Experimental data sets were modeled by applying two different schemes of relaxation pathways of (9,7)-SWNTs after photoexcitation. This material is available free of charge via the Internet at http://pubs.acs.org.

AUTHOR INFORMATION

Corresponding Author

*E-mail: manfred.kappes@kit.edu; andreas.unterreiner@kit.edu.

■ ACKNOWLEDGMENT

This work was supported by the Deutsche Forschungsgemeinschaft (DFG) and the State of Baden-Württemberg through the DFG-Center for Functional Nanostructures (CFN) within subproject C3.02.

■ REFERENCES

(1) Lauret, J.-S.; Voisin, C.; Cassabois, G.; Delalande, C.; Roussignol, Ph.; Jost, O.; Capes, L. *Phys. Rev. Lett.* **2003**, *90*, 57404.
(2) Deria, P.; Sinks, L. E.; Park, T.-H.; Tomezsko, D. M.; Brukman, M. J.; Bonnell, D. A.; Therien, M. J. *Nano Lett.* **2010**, *10*, 4192.
(3) Yang, J.-P.; Kappes, M. M.; Hippler, H.; Unterreiner, A.-N. *Phys. Chem. Chem. Phys.* **2005**, *7*, 512.
(4) Huang, L.-B.; Pedrosa, H. N.; Krauss, T. D. *Phys. Rev. Lett.* **2004**, *93*, 17403.
(5) Carlson, L. J.; Krauss, T. D. *Acc. Chem. Res.* **2008**, *41*, 235.
(6) Torrens, O. N.; Zheng, M.; Kikkawa, J. M. *Phys. Rev. Lett.* **2008**, *101*, 157401.
(7) Lüer, L.; Gadermaier, C.; Crochet, J.; Hertel, T.; Brida, D.; Lanzani, G. *Phys. Rev. Lett.* **2009**, *102*, 127401.
(8) Nish, A.; Hwang, J.-Y.; Doig, J.; Nicholas, R. J. *Nat. Nanotechnol.* **2007**, *2*, 640.
(9) Lebedkin, S.; Hennrich, F.; Kiowski, O.; M. Kappes, M. *Phys. Rev. B* **2008**, *77*, 165429.
(10) O'Connell, M. J.; Bachilo, S. M.; Huffman, C. B.; Moore, V. C.; Strano, M. S.; Haroz, E. H.; Rialon, K. L.; Boul, P. J.; Noon, W. H.; Kittrell, C.; Ma, J.; Hauge, R. H.; Weisman, R. B.; Smalley, R. E. *Science* **2002**, *297*, 593.
(11) Lee, A. J.; Wang, X.; Carlson, L. J.; Smyder, J. A.; Loesch, B.; Tu, X.; Zheng, M.; Krauss, T. D. *Nano Lett.* **2011**, *11*, 1636.
(12) Tretiak, S. *Nano Lett.* **2007**, *7*, 2201.
(13) Zhao, H.; Mazumdar, S.; Sheng, C.-X.; Tong, M.; Vardeny, Z. V. *Phys Rev. B* **2006**, *73*, 075403.
(14) Perebeinos, V.; Tersoff, J.; Avouris, P. *Phys. Rev. Lett.* **2005**, *94*, 027402.
(15) Srivastava, A.; Htoon, H.; Klimov, V. I.; Kono, J. *Phys. Rev. Lett.* **2008**, *101*, 087402.
(16) Matsunaga, R.; Matsuda, K.; Kanemitsu, Y. *Phys. Rev. B* **2010**, *81*, 033401.
(17) Ghosh, S.; Bachilo, S. M.; Simonette, R. A.; Beckingham, K. M.; Weisman, R. B. *Science* **2010**, *330*, 1656.
(18) Kiowski, O.; Arnold, K.; Lebedkin, S.; Hennrich, F.; Kappes, M. M. *Phys. Rev. Lett.* **2007**, *99*, 237402.
(19) Lebedkin, S.; Schweiß, P.; Renker, B.; Malik, S.; Hennrich, F.; Neumaier, M.; Stoermer, C.; Kappes, M. *Carbon* **2002**, *40*, 417.
(20) Lebedkin, S.; Arnold, K.; Hennrich, F.; Krupke, R.; Renker, B.; Kappes, M. M. *New J. Phys.* **2003**, *5*, 140.
(21) Stürzl, N.; Hennrich, F.; Lebedkin, S.; Kappes, M. M. *J. Phys. Chem. C* **2009**, *113*, 14628.
(22) Hagen, A.; Steiner, M.; Raschke, M. B.; Lienau, C.; Hertel, T.; Qian, H.; Meixner, A. J.; Hartschuh, A. *Phys. Rev. Lett.* **2005**, *95*, 197401.
(23) Valkunas, L.; Ma, Y.-Z.; Fleming, G. R. *Phys. Rev. B* **2006**, *73*, 115432.
(24) Lüer, L.; Hoseinkhani, S.; Polli, D.; Crochet, J.; Hertel, T.; Lanzani, G. *Nature Phys.* **2009**, *5*, 54.
(25) Ma, Y.-Z.; Valkunas, L.; Dexheimer, S. L.; Bachilo, S. M.; Fleming, G. R. *Phys. Rev. Lett.* **2005**, *94*, 157402.
(26) Plentz, F.; Ribeiro, H. B.; Jorio, A.; Strano, M. S.; Pimenta, M. A. *Phys. Rev.* **2005**, Lett. *95*, 247401.
(27) Chou, S. G.; Plentz, F.; Jiang, J.; Saito, R.; Nezich, D.; Ribeiro, H. B.; Jorio, A.; Pimenta, M. A.; Samsonidze, G. G.; Santos, A. P.; Zheng, M.; Onoa, G. B.; Semke, E. D.; Dresselhaus, G.; Dresselhaus, M. S. *Phys. Rev. Lett.* **2005**, *94*, 127402.
(28) Hippler, H.; Unterreiner, A.-N.; Yang, J.-P.; Lebedkin, S.; Kappes, M. M. *Phys. Chem. Chem. Phys.* **2004**, *6*, 2387.
(29) Perebeinos, V.; Tersoff, J.; Avouris, P. *Phys. Rev. Lett.* **2005**, *94*, 027402.
(30) Plentz, F.; Ribeiro, H. B.; Jorio, A.; Strano, M. S.; Pimenta, M. A. *Phys. Rev. Lett.* **2005**, *95*, 247401.
(31) Ostojic, G. N.; Zaric, S.; Kono, J.; Moore, V. C.; Hauge, R. H.; Smalley, R. E. *Phys. Rev. Lett.* **2005**, *94*, 097401.
(32) Zhu, Z.; Crochet, J.; Arnold, M. S.; Hersam, M. C.; Ulbricht, H.; Resasco, D.; Hertel, T. *J. Phys. Chem. C* **2007**, *111*, 3831.
(33) Jones, M.; Metzger, W. K.; McDonald, T. J.; Engtrakul, C.; Ellingson, R. J.; Rumbles, G.; Heben, M. J. *Nano Lett.* **2007**, *7*, 300.
(34) Carlson, L. J.; Krauss, T. D. *Acc. Chem. Res.* **2008**, *41*, 235.
(35) Gao, J.; Loi, M. A. *Eur. Phys. J. B* **2010**, *75*, 121.
(36) Huang, L.; Pedrosa, H. N.; Krauss, T. D. *Phys. Rev. Lett.* **2004**, *93*, 017403.
(37) Perebeinos, V.; Tersoff, J.; Avouris, P. *Phys. Rev. Lett.* **2004**, *92*, 257402.
(38) Perebeinos, V.; Tersoff, J.; Avouris, P. *Nano Lett.* **2005**, *5*, 2495.
(39) Spataru, C. D.; Ismail-Beigi, S.; Capaz, R. B.; Louie, S. G. *Phys. Rev. Lett.* **2005**, *95*, 247402.
(40) Zhao, H.; Mazumdar, S. *Phys. Rev. Lett.* **2004**, *93*, 157402.
(41) Scholes, G. D.; Tretiak, S.; McDonald, T. J.; Metzger, W. K.; Engtrakul, C.; Rumbles, G.; Heben, M. J. *J. Phys. Chem. C* **2007**, *111*, 11139.
(42) Kilina, S.; Badaeva, E.; Piryatinski, A.; Tretiak, S.; Saxena, A.; Bishop, A. R. *Phys. Chem. Chem. Phys.* **2009**, *11*, 4113.
(43) Murakami, Y.; Lu, B.; Kazaoui, S.; Minami, N.; Okubo, T.; Maruyama, S. *Phys. Rev. B* **2009**, *79*, 195407.
(44) Santos, S. M; Yuma, B.; Berciaud, S.; Shaver, J.; Gallart, M.; Gilliot, P.; Cognet, L.; Lounis, B. *Phys. Rev. Lett.* **2011**, *107*, 187401.
(45) Matsunaga, R.; Matsuda, K.; Kanemitsu, Y. *Phys. Rev. Lett.* **2011**, *106*, 037404.
(46) Styers-Barnett, D. J.; Ellison, S. P.; Mehl, B. P.; Westlake, B. C.; House, R. L.; Park, C.; Wise, K. E.; Papanikolas, J. M. *J. Phys. Chem. C* **2008**, *112*, 4507.
(47) (a) Harutyunyan, H.; Gokus, T.; Green, A. A.; Hersam, M. C.; Allegrini, M.; Hartschuh, A. *Phys. Stat. Sol. B* **2009**, *246*, 2679. (b) Harutyunyan, H.; Gokus, T.; Green, A. A.; Hersam, M. C.; Allegrini, M.; Hartschuh, A. *Nano Lett.* **2009**, *9*, 2010.